PROCEEDINGS, 41st Workshop on Geothermal Reservoir Engineering
Stanford University, Stanford, California, February 22-24, 2016
SGP-TR-209

Fracture and Flow System Modeling Method for an EGS Reservoir

George Danko[1*], Davood Bahrami[1], Ivan Vazquez[1]

[1] University of Nevada, Reno

[*]Corresponding Lead Author: danko@unr.edu

Keywords: Fracture network, thermo-hydraulic-mechanic model, inverse property identification

ABSTRACT

A modeling method comprising four phases is proposed to evaluate an as-created EGS reservoir. The first step is to process the Micro-EarthQuake (MEQ) location data obtained during reservoir creation in the 3-D visual environment of AutoCAD. Each hydrofracturing event results in a specific set of MEQ locations forming a cloud of recognizable, 3-D ellipsoid shape. The second step is to visually match each 3-D ellipsoid MEQ cloud with a 2-D, planar ellipsis with strike and dip orientations and lateral, principal diameters in the fracture plane in AutoCAD. In the same step, a planar discretization mesh is added inside the ellipses. The position and the length of the connecting intersections between the neighboring fractures can be adjusted in the visual environment to match model outcome against field observation. Connections and intersections with the injection and production boreholes are also added to form a 3-D mesh system for the reservoir. The third step is the creation of the circulation fluid flow network model by defining planar flow channels along the mesh edges as branch connections. The hydraulic aperture of each branch is defined as a function of the thermo-mechanical-chemical response of the rock strata around the hydraulic system of the fracture network. The fourth step is to solve the coupled T-H-M-C network model numerically and to match the model results with the measurement data obtained from field tests. Particularly, fluid circulation flow and pressure loss experiment defined by steady-state flow test; and thermal drawdown measured over several weeks or months must be matched, minimizing deviation between model and measurement data. During minimization, the T-H-M-C model parameters, especially fracture aperture properties, are varied for achieving a best fit.

The method is demonstrated for the Fenton Hill, Phase II reservoir using the published data for the microseismic active planes obtained from the Massive Hydraulic Fracturing Experiment #2032 and the fluid circulation experiments defined as Experiment #2067. A simple fracture aperture model is identified, shown to be able to characterize the Phase II reservoir circulation flow against measured data obtained during field tests.

1. INTRODUCTION

Engineered geothermal reservoirs are developed by artificial fracture creation or by the stimulation and connection of existing natural fractures. Large, connected fractures are essential for providing fluid transport and convective heat exchange with the hot host rock of the reservoir. Hydrofracturing or fracture stimulation is the main, first step for the creation of a geothermal reservoir. The next most important task is to test the connected fracture system for substantial volume and heat transfer area. The evaluation of the resultant EGS reservoir regarding its actual size, pumpability, and energy capacity requires circulation experiments, flow, pressure, and temperature measurements and descriptive T-H-M-C model studies.

An adept reservoir simulation model is expected to capture the reservoir's main characteristics obtained from field measurements, especially regarding its circulation flow resistance and thermal drawdown as a function of injection time. The Fenton Hill Phase I and Phase II EGS reservoir research studies provide a rich, well-documented set of field data for matching with descriptive T-H-M-C models. Using the results conducted at the Los Alamos National Laboratory (LANL) between 1978 and 1995 (published by Murphy et al, 1981; Smith et al, 1989; and DOE, 2006), two challenge problems are defined. Various modeling approaches and simulation codes are used in the Code Comparison Study (GTO-CCS) tasks as part of the US Department of Energy (DOE) Geothermal Technologies Office (GTO) program.

This paper addresses a new model setup method and the initial flow model of the complex Challenge Problem 1, using the geometry, input properties, and measurement data from the published Fenton Hill Phase II experiments (Smith et al, 1989). For the MEQ clouds, the experimental data obtained during the Massive Hydraulic Fracturing (MHF) experiment #2032 are used, originating from Smith et al. (1989). The MEQ data set is used in the paper to validate the new model setup method for identifying the position, orientation, and lateral dimensions of 10 major, planar fractures, using AutoCAD (AutoCAD, 1982).

The coupled, T-H-M-C network model, reduced for the present studies for only the H-M model part, is set up in MULTIFLUX (Danko, 2008). The reference measurement data set for the circulation flow and pressure variations with time is taken from the fluid circulation experiments conducted at Fenton Hill, defined as RVFT (Duchane, 1966). The hydraulic fracture aperture model follows the H-M coupling element published for the Fenton Hill phase I study (Danko and Bahrami, 2013a, 2013b). The goal of the study is to match the numerical model results with the measured pressure and fluid circulation flow rate data by varying only two unknown model parameters, defined as initial fracture aperture, δ_0, and the pressure coefficient, C^P, common for all ten planar fractures in the exercise.

2. THE GEOMETRY OF THE EGS RESERVOIR AT FENTON HILL PHASE II

The conceptual design of the massive fracture system at Fenton Hill Phase II is shown in Figure 1a., drawn after Smith et al. (1989). The as-created fracture system can only be guessed from the MEQ cloud data obtained during various hydrofracturing events as well as from the survey data for the wells.

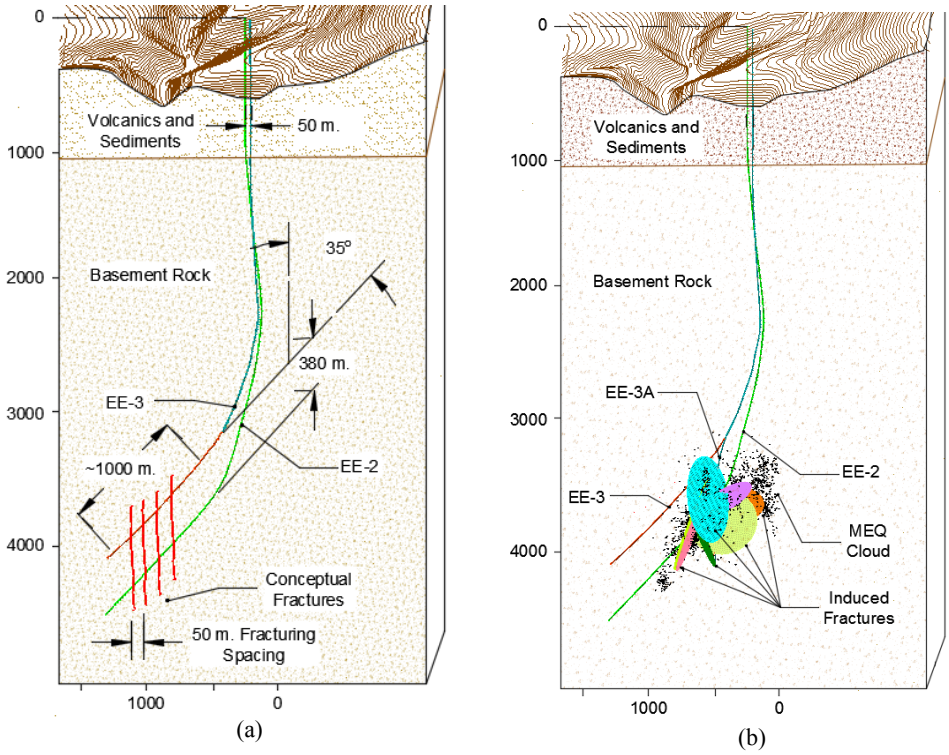

Figure 1. Conceptualized schematic of the Fenton Hill Phase II (Source: Smith et al., 1989), (a); and the MEQ cloud and induced fractures obtained by hydrofracturing, (b).

The MEQ locations have been analyzed by researchers in order to characterize the reservoir volume as well as the geometry of the created or stimulated fractures documented as Experiment #2032 (Smith et al., 1989). The authors identified 10 major fracture planes using the three-point location method of clustering the MEQs. Another method called the Waveform Amplitude Ratios in the literature may also be used to identify fractures by clustering the seismic cloud (Roff et al., 1996) using the similarity in S/P ratio and spatial proximity between the MEQs. The identified fracture planes by Smith et al., (1989) were used for convenience with published strike and dip data. The MEQ cloud's source is shown Fig. 1b together with the 10 identified fractures. As shown, the MEQ cloud in Fig. 1b does not follow the target area in Fig. 1a. A new section of a well, EE-3A had to be drilled from EE-3 to create an injection well for fluid circulation via EE-2.

Each of the 10 fractures is manually adjusted with its elliptical size and location in AutoCAD until good visual match is obtained placing the planar fracture within the corresponding seismic sub-cloud. The process of fracture network validation includes comparing the fluid flow rate between the intersected fractures using published data (Smith et al., 1989) shown in Figure 2. There are 19 connecting intersections between the 10 planar fractures. The strength of flow connections between the corresponding fractures listed in Table 1 is proportional to the length of the intersection lines between connected fractures. A normalized length of each intersection line is calculated by dividing with the shortest length of the lines. The size and location of each of the 10 fractures are adjusted for best match. The agreement between the published connectivity, also normalized by the line thickness ratio from the published data, is shown in Figure 3. Table 1 summarizes the results of the identified fractures for best match with the published connectivity, achieving a correlation of 0.93. Figure 4 shows the 3D view of the MEQ clouds, the fractures as well as the injection and production wells. Figure 5 depicts the intersections of the fractures with boreholes EE-2 and EE-3A. The identified set of fractures from this process matches closely most part of the MEQ cloud. However, some parts of the MEQ clouds are left out as remote areas not connected to the wells. These dead-end fracture areas may add reservoir volume but likely stay out of the circulation flow paths. The fracture network with the injection and production wells are also included in the H-M model setup reported in the paper.

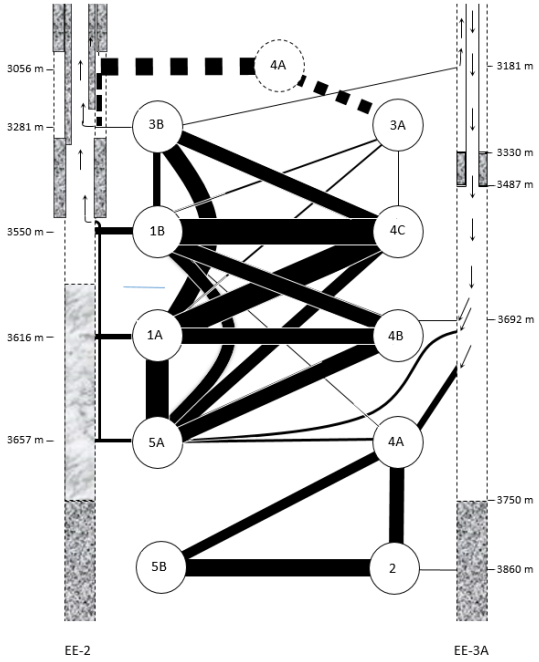

Figure 2. Schematic showing the intersections between the various fractures during the ICFT (Experiment 2067) (Source: Smith et al., 1989).

Table 1. Idealized fractures of Fenton Hill II with the identified location, lateral fracture size and mesh size obtained in AutoCAD.

			Centroid Location			CCW Direction		Strike	Dip	Mesh Size
Code	Radius R [m]	Radius r [m]	X	Y	Z (TVD)	Z	Y			(m^2)
1-A	310	283	-440	-32	3371	29	-76	N29W	76E	16
1-B	320	260	-456	-34	3381	29	-76	N29W	76E	16
2	200	80	-296	-483	3707	-88	-153	N88E	27W	10
3-A	175	40	-435	-133	3561	29	-113	N29W	67W	9
3-B	215	120	-294	-406	3601	29	-113	N29W	67W	14
4-A	215	120	-294	-406	3601	-6	-67	N6E	67E	11
4-B	170	90	-361	-287	3401	-5	-64	N5E	64E	9
4-C	220	165	-418	-285	3364	-8	-67	N8E	67E	11
5-A	205	190	-380	-338	3545	-33	-120	N33E	60W	10
5-B	170	110	-260	-562	3606	-34	-124	N34E	56W	9

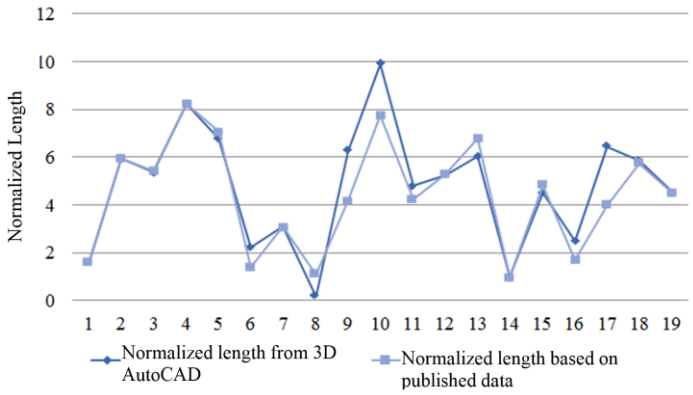

Figure 3. Comparison of the normalized fracture connections between published data and current 3D AutoCAD.

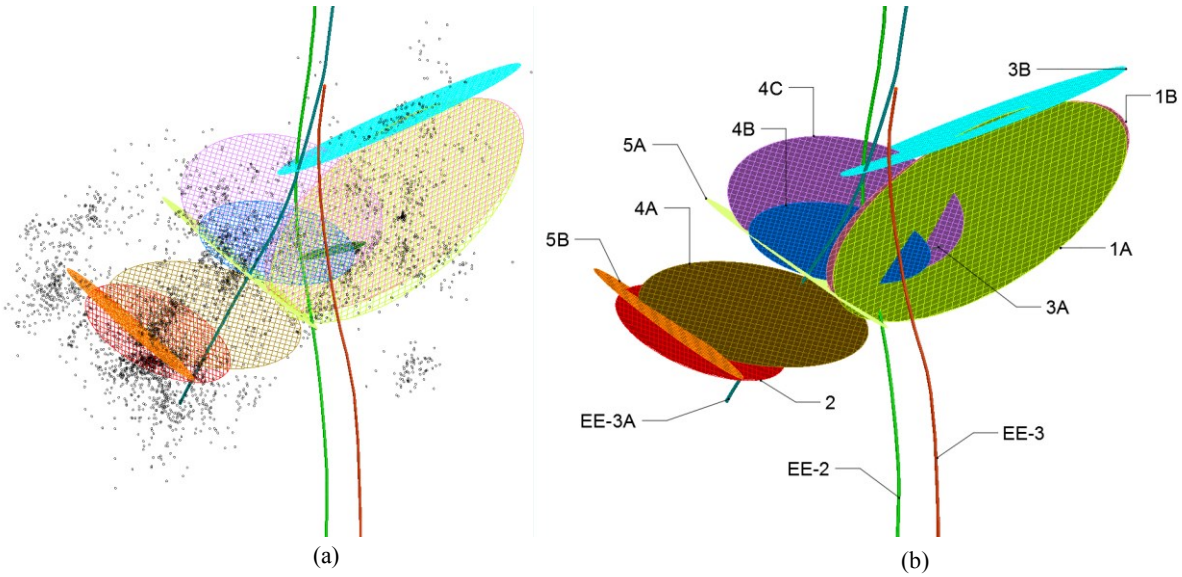

(a) (b)

Figure 4. Perspective view of the constructed fracture network with the overlaid MEQs, (a); and the planar fractures without the MEQs, (b).

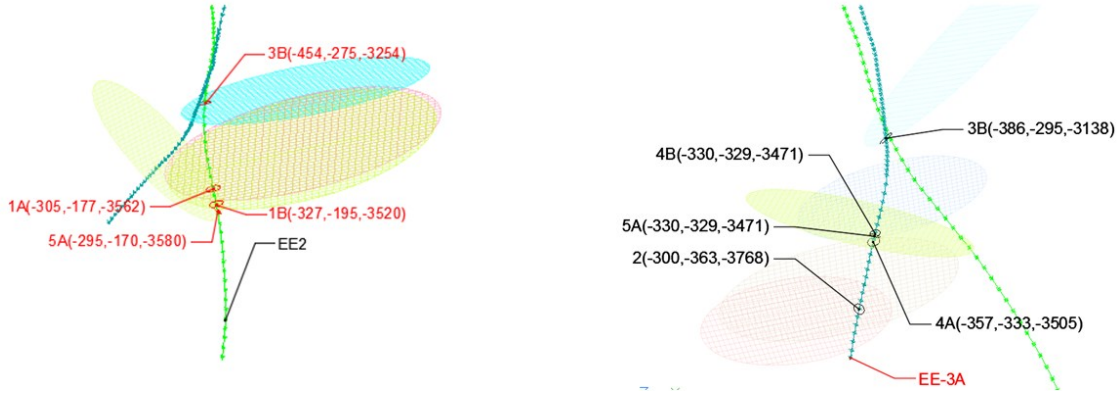

(a) (b)

Figure 5. Location of the fracture-well intersections of the fractures with borehole EE-2, (a); and with borehole EE-3A, (b).

Table 2. Coordinates of the intersection points between the fractures and the EE2 and EE-3A boreholes.

	Intersection with Wellbore EE-2				Intersection with Wellbore EE-3A		
Fracture	X	Y	Z	Fracture	X	Y	Z
3B	-454	-275	-3254	3B	-386	-295	-3138
1A	-305	-177	-3562	2	-300	-363	-3768
1B	-327	-195	-3520	4A	-327	-333	-3505
5A	-295	-170	-3580	4B	-330	-329	-3471
				5A	-330	-330	-3480

3. THE FRACTURE FLOW NETWORK

Each single fracture is divided into square mesh elements defining planar channels along the mesh edges as branch connections, shown in Figure 6a. The hydraulic aperture of the branch modeling a fracture section is defined in general as a function of the thermo-mechanical-chemical response of the rock strata to the changes in the flow system in the fracture network. The hydraulic diameter of each flow channel is determined as follows:

$$D_h = \frac{4A}{Per} = \frac{4\delta W}{2W} = 2\delta \tag{1}$$

In the Eq.(1), δ is the fracture aperture and W is the mesh size. The flow network is solved in MULTIFLUX for the unknown nodal fluid pressure and velocity in each pixel. The simple fracture flow network for all 10 fractures together with part of the injection and production wells are shown in Figure 6b. The fracture model is used to determine the fracture aperture as a function of fluid pressure and temperature, described in the next section.

4. THE FRACTURE APERTURE MODEL

Fracture aperture is the most important element of the EGS model as it greatly affects the flow resistance and in turn the flow distribution which affects the energy extraction from the host rockmass. Two fracture aperture models are used in MULTIFLLUX (Danko and Bahrami, 2013a, 2013b). The first is a simple, linear, compressive mechanical model with the thermal contraction included without any neighbor effect between the fracture mesh elements as follows:

$$\delta_i = \delta_0 + C^p[P_i - P_0] + C^T\left[[\overline{\Delta L}]\right][T_i - T_0] \tag{2}$$

The C^p, and C^T are pressure and thermal aperture coefficients, respectively. The $C^T\left[[\overline{\Delta L}]\right][T_i - T_0]$ term is the functional form of the host rock thermal contraction with T_i being the fracture wall temperature and T_0 being the in situ host rock temperature at the given grid location on the fracture plane. The thermal contraction function is an abstraction of a time-dependent element which is obtained through a novel methodology called Numerical Transport Code Functionalization (NTCF) developed by Danko (2006). The host rock model is abstracted using the NTCF model identification procedure, performing a single run of a porous media code capable of solving heat flow such as NUFT (Nitao, 2000) or TOUGH (Pruess et al., 1999). The thermal layer penetration depth from the fracture surface into the host rock is a time-dependent variable. The thermal contraction of each fracture element is calculated from the variable temperature profile obtained from the NTCF model element and the linear thermal expansion coefficient.

The thermal aperture coefficient, C^T, is assumed to be zero in this paper for the sake of simplicity. The full, time-dependent model results with thermal contraction included is work in progress. The simple, compression-only aperture model assumes no neighbor effect between the fracture elements in terms of mechanical opening. However, a more detailed fracture model (Danko and Bahrami, 2013a, 2013b) describes the opening of each fracture element as constrained by the shear stress connection between the neighbor elements, as shown in Figure 7. The matrix-vector model for the combined shear-stress and compression fracture aperture model is given as follows:

$$[\delta_i] = \delta_0 + \left[[R_{C^P}]\right]^{-1} \cdot \left([P_i - P_0] + C^T\left[[\overline{\Delta L}]\right][T_i - T_0]\right) \tag{3}$$

where the $\left[[R_{C^P}]\right]$ matrix is composed from the shear and compression resistances in an n x n array.

It is known that the fracture aperture models are nonlinear with respect to fluid pressure. The fracture aperture model in Eq. (3) is based on the assumption of sectional linearization over the applicable pressure regime. A nonlinear response of a fracture or joint can be captured as incremental variation starting from the initial parameters of pressure, P_0, and aperture, δ_0, of the linearized fracture model.

The combined shear and compression fracture aperture model applied to a single 200 m diameter fracture with one injection and one production points is used for the demonstration of fracture opening. The fracture mesh and the aperture distribution are shown in Figure 8, depicting a lens-shaped fracture as a result. However, a simple penny-shape fracture aperture is assumed in the current exercise to first match the measured circulation data. The variable fracture aperture model is a study in progress.

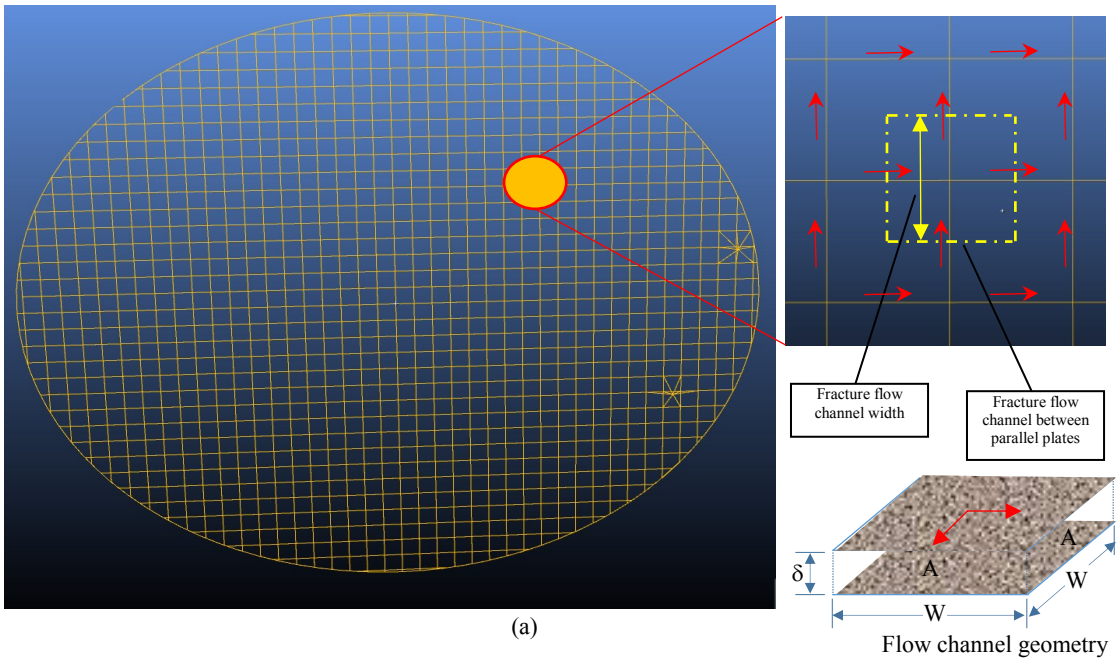

Figure 6. Fracture flow network mesh for single planar fracture.

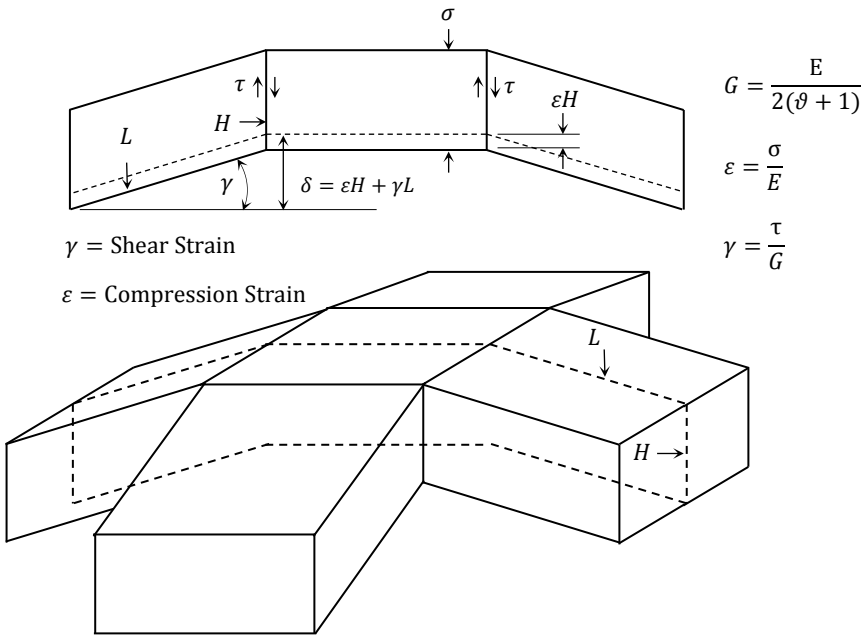

Figure 7. Compression and no-slip shear deformations in the continuum rock around a planar fracture.

5. IDENTIFICATION OF THE FRACTURE APERTURE FROM MATCHING WITH MEASUREMENT

For testing the fracture flow network model, the steady-state production segment data of the Fenton Hill Phase II (Duchane, 1996), Reservoir Verification Flow Test (RVFT) is used to first characterize the reservoir fracture network pressure parameter, C^P, by matching and then simulating the flow through the system. The operational stages of the RVFT with time are shown in Figure 9. The reservoir operating conditions during Stages 1 and 2 of the RVFT are summarized in Table 3.

Table 3. The reservoir operating conditions during stages 1 and 2 of the RVFT (Source: Duchane, 1996)

	Stage 1 (May 1995)	Stage 2 (June 1995)
Injection:		
Flow rate, gpm (L/s)	127 (8.0)	120 (7.6)
Pressure, psi (MPa)	3960 (27.3)	3960 (27.3)
Production:		
Flow rate, gpm (L/s)	105 (6.6)	94 (5.9)
Pressure, psi (MPa)	1400 (9.7)	2200 (15.2)
Temperature, (^{o}C)	184	181
Circulation driving pressure, psi (MPa)	2560 (17.7)	1760 (12.1)

A trial-and-error procedure is used to identify the average fracture aperture, uniform for all 10 planar fractures in the flow system which includes the injection and extraction wells. The production pressure is used as the given backpressure and the production flow rate as a given boundary condition, neglecting the water loss from system in this study. While keeping the boundary conditions during each stage of the operation constant, the fracture aperture is varied until the injection pressure from the simulation matches the measured injection pressure from the RVFT. Two different average aperture values are obtained for the two stages as: δ_1=0.094 mm, and δ_2=0.103 mm, giving perfect match for the injection pressure for Stages 1 and 2, respectively. The reservoir-level fluid pressure is estimated assuming an average depth of 3400 m and average reservoir hydrostatic pressure of 34 MPa.

The estimated reservoir operating conditions at the reservoir level for Stages 1 and 2 are summarized in Table 4 together with the matched average fracture aperture. The pressure coefficient and the initial aperture of the fractures are determined from Eq. (2) by solving it as a set of two equations for two reservoir operating conditions with C^T=0 as follows:

$$\left.\begin{aligned}\delta_1 &= \delta_0 + C^p(P_1 - P_0)\\ \delta_2 &= \delta_0 + C^p(P_2 - P_0)\end{aligned}\right\} \tag{4}$$

Substituting δ_1=0.094 mm; δ_2=0.103 mm; P_0=34 MPa; P_1=52.5 MPa; and P_2=55.25 MPa, the solution gives δ_0 = 0.0335 mm and C^p=3.2727x10^{-12} m/Pa.

Table 4. The estimated reservoir operating conditions during stages 1 and 2 of the RVFT.

	Production rate	Hydrostatic Pressure at 3400 m average depth	Injection Pressure at surface	Production Pressure at surface	Average pressure at reservoir level	Driving pressure at surface	Fracture Aperture
	(L/s)	(MPa)	(MPa)	(MPa)	(MPa)	(MPa)	mm
Stage 1	6.6	34	27.3	9.7	52.5	17.7	0.094
Stage 2	5.9	34	27.3	15.2	55.25	12.1	0.103

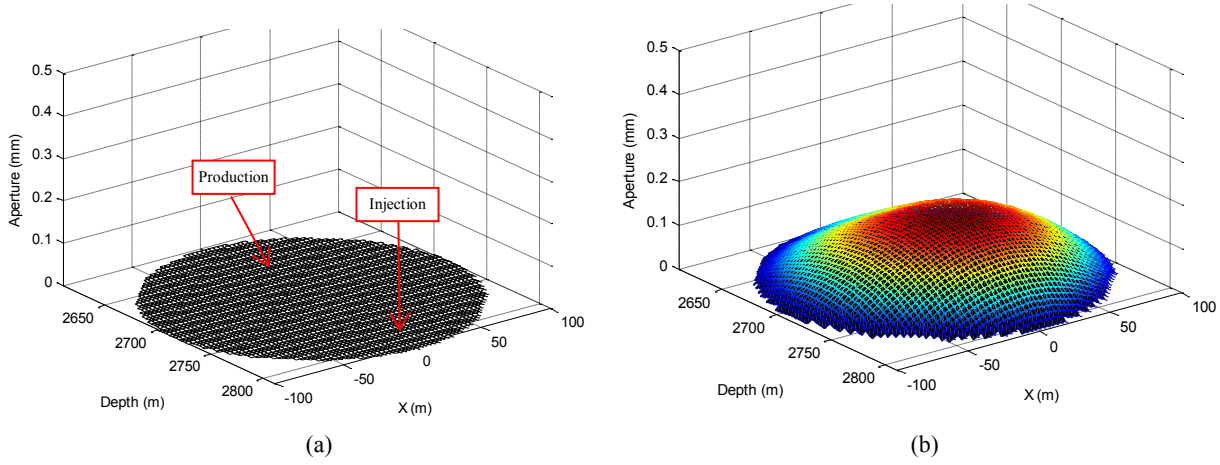

Figure 8. Flow mesh of a single fracture of 200 m in diameter, (a); and the fracture aperture distribution in (mm) using the combined shear-compression, variable aperture model for an injection pressure of 9 MPa, (b).

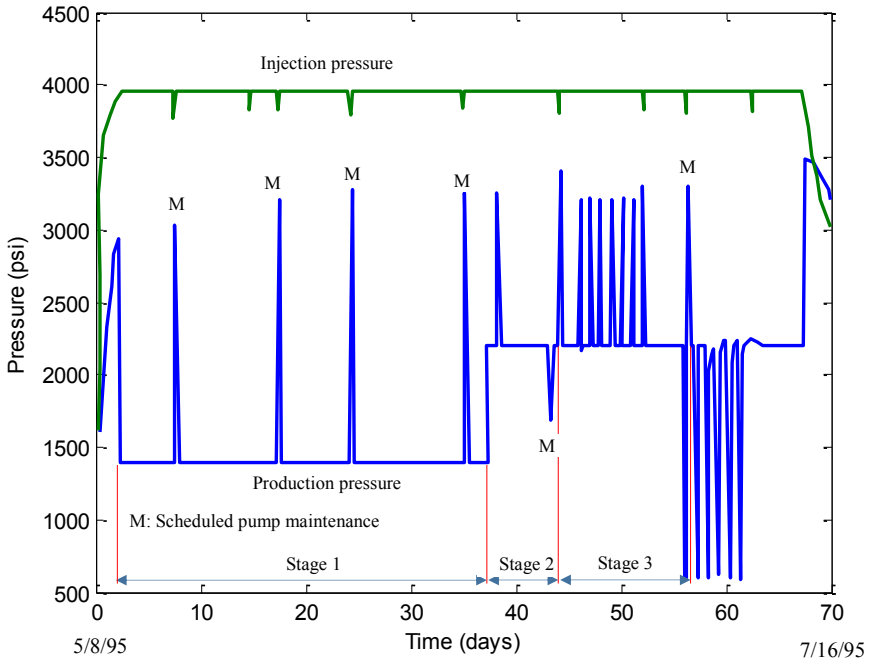

Figure 9. Operational stages of the steady-state production segment (RVFT), May 10-July 14, 1995 (Source: Duchane, 1996, third production segment, pages 4.225-4.228).

6. FLOW MODEL RESULTS AND DISCUSSION

The calibrated penny-shape apertures for Stages 1 and 2 of the RVFT measurement with 6.6 L/s and 5.9 L/s are used to solve the reservoir fracture network model. The matched parameter, C^P=3.2727x10^{-12} m/Pa, is in reasonable agreement with the value obtained for Fenton Hill Phase I of C^P=4.48x10^{-12} m/Pa (Danko and Bahrami, 2013a). The mass flow rate distributions in the fracture system for the Stages 1 and 2 of the RVFT measurement are shown in Figure 10. The flow distribution is highly variable due to multiple intersections between the fractures but very similar for the two stages confirming that the penny-shape assumption is not responsive to different operating conditions in terms of active surface flow areas. The injection pressure is kept constant, 27.3 MPa, during the measurement of RVFT. The production pressure, on the other hand, is 9.7 MPa, and 15.2 MPa for stages 1 and 2, respectively. The driving pressure defined as the difference between the production and injection pressures are 17.7 MPa and 12.1 MPa for stages 1 and 2, respectively, giving corresponding fracture apertures of 0.094 mm and 0.103 mm. The larger average fracture aperture for the larger back pressure can be attributed to the higher pressure on the fracture wall causing larger fracture opening.

Several simplifications are made in the presented model with penny-shape fractures, average apertures, and constant temperatures. In reality, spatially lens-shape fractures will develop as the planar fractures interact with the host rock, described by Eq. (3) and illustrated in Figure 8. Such a model is computationally intensive to solve for unknown δ_o and C^P, requiring the solution of large matrix equations iteratively for all 10 planar fractures since the pressure coefficient, C^P, is an input parameter for the $[[R_{C^P}]]^{-1}$ inverse matrix. The task can now progress into this phase starting with the average δ_o and C^P values from the approximate solution.

Furthermore, in reality, the constant fluid temperature assumption which holds very well for Stages 1 and 2 from measurement does not mean constant thermal contraction condition in the host rock. A refined model matching exercise must include the thermal contraction element with non-zero C^T thermal coefficient in Eq. (3). Therefore, this task adds another trial-and-error model matching iteration loop to the inverse solution. The fracture aperture would likely increase in all active fracture areas with the progressing circulation time as it is manifested in the improved impedance of the system with time, requiring an increased back pressure in stage 2 relative to stage 1.

It is interesting to observe that the measured production rate decreased with the increased back pressure while the production temperature is also decreased. The trend signifies a decrease in extracted thermal energy with time, indicating rock cooling that must result in thermal contraction and fracture opening. Therefore, the fracture apertures will not stay uniform neither spatially nor temporally in the refined model with C^T and C^P both present. Likewise, the flow field distribution will be more responsive to the flow rate increase, opening more flow paths in the fracture plane, reflecting larger thermal surface area with higher back pressure. It is expected that the complete model will match the trend of the measured thermal drawdown.

5. CONCLUSIONS AND RECOMMENDATIONS

It is demonstrated that the model of a large network of fractures in Fenton Hill Phase II reservoir can be set up and solved for the flow distribution successfully.

It is shown that the model can be calibrated for fracture flow against field measurements using a simple fracture aperture model with only two joint model parameters which can be both identified from data obtained during circulation tests of two different operation stages.

The δ_0 and C^P planar fracture parameters are very similar in numerical values to those obtained for the published planar fracture model for Fenton Hill, Phase I.

A more advanced fracture model can also be applied assuming variable fracture aperture of lens-shape fracture profile and thermal contraction. Such a model is expected to be predictive for the thermal drawdown and responsive to the changes in the injection flow rate in terms of fracture flow distribution.

ACKNOWLEDGEMENTS

The U.S. Department of Energy is acknowledged for the financial support for the study. The effort of the office of the code comparison studies, Pacific Northwest National Laboratory and especially Dr. Mark White and Ms. Signe White for managing the Velo site are also thankfully acknowledged.

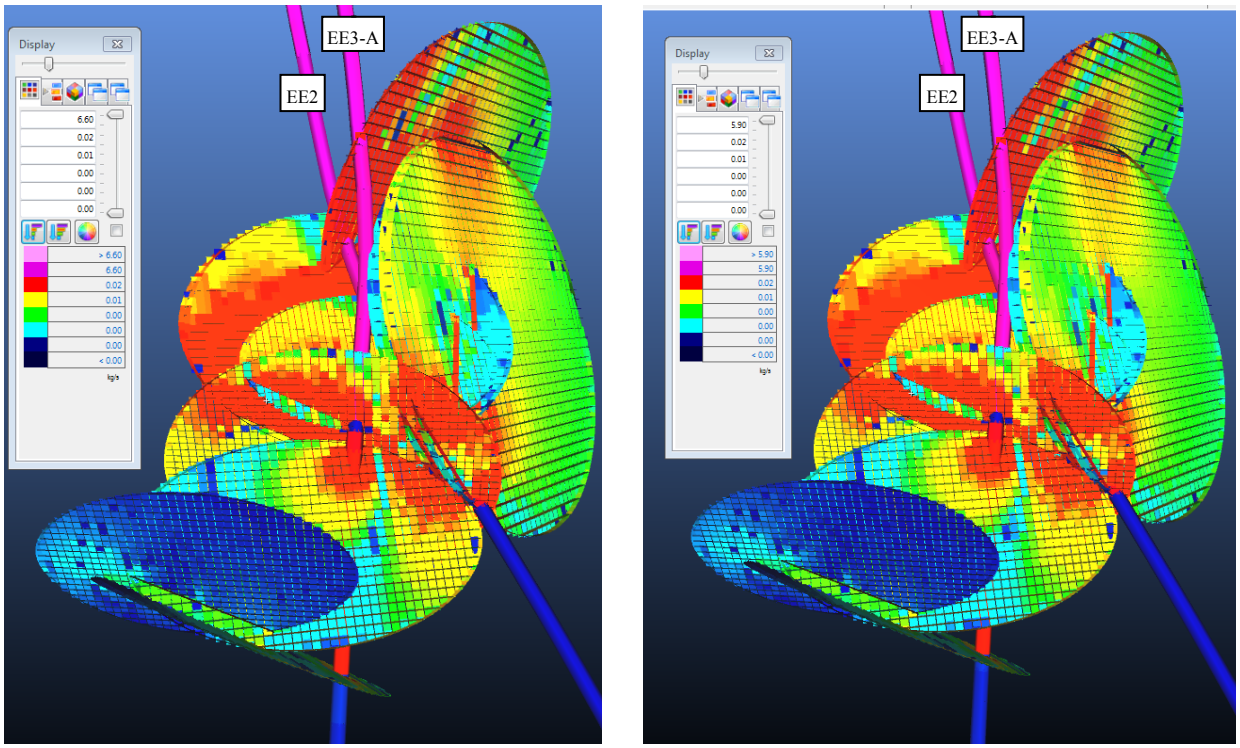

(a) (b)

Figure 10. Simulated flow distribution in the Fenton Hill Phase II, stage 1, (a); and stage 2 ,(b) of the RVFT.

REFERENCES

Danko, G. and Bahrami, D.: Dynamic Model of Discrete Fracture Opening Under Fluid Injection. *Proceedings, Thirty-Eighth Workshop on Geothermal Reservoir Engineering, Stanford University, Stanford, California, February 11-13*, (2013a), 395-404.

Danko G. and Bahrami D.: EGS Model Adaptation and Forecasting Studies with MULTIFLUX. *Geothermal Resources Council 2013 Annual Meeting, Las Vegas, Nevada,* 36, (2013b), 141-147.

Murphy, H., Tester, J., Grigsby C., and Potter, R.: Energy Extraction from Fractured Geothermal Reservoirs in Low Permeability Crystalline Rock. *Journal of Geophysical Research*, 86, B8, (1981), 7145-7158.

Danko, G.: Functional or Operator Representation of Numerical Heat and Mass Transport Models. *ASME J. of Heat Transfer,* vol. 128, (2006) pp. 162-175.

Danko, G.: MULTIFLUX V5.0 Software Documentation Qualification Documents, Software Tracking Number: 1002-5.0-00, *Software Management Office, Berkeley National Laboratory*. (2008)

Department Of Energy: History of Geothermal Energy Research and Development in the United States, Reservoir Engineering 1978-2006. *Geothermal Technology Program*, pp. 59-61.

Duchane, D. V.: Heat mining to extract hot dry rock geothermal energy: technical and scientific progress. *Federal Geothermal Research Program Update, Fiscal Year 1995, U.S. Department of Energy, Washington, DC*, (1996) pp, 4.215–4.230.

Roff A., Phillips W. S., and Brown D. W.: Joint Structures Determined by Clustering Microearthquakes Using Waveform Amplitude Ratios. *International Journal of Rock Mechanics and Mining Sciences and Geomechanics Abstracts*. Vol. 33, No. 6, (1996), pp. 627-639.

Smith, M. C., Hendron, R. H., Murphy, H. D., & Wilson, M. G.: Hot Dry Rock Geothermal Energy Development Program. *Annual Report, Fiscal Year 1987. Los Alamos National Laboratory, New Mexico*, (1989).

Pruess, K., Oldenburg C., and Moridis G.: TOUGH2 User's Guide, Version 2.0. *Report LBNL-43134, Lawrence Berkeley National Laboratory, Earth Sciences Division, Berkeley, California*, (1999).

Nitao, J.: NUFT, Flow and Transport code V3.0. *Software Configuration Management, Yucca Mountain Project – STN: 10088-30S00, Prepared at the Lawrence Livermore National Laboratory,* (2000).

AutoCAD, Computer Aided Design, *Autodesk, Mill Valley California, CA*, (2015).